THE JOURNAL OF PHYSICAL CHEMISTRY C

Article

Cite This: J. Phys. Chem. C 2019, 123, 1839−1845

pubs.acs.org/JPCC

Self-Encapsulation of Silicene in Cubic Diamond Si: Topological Semimetal in Covalent Bonding Networks

Geun-Myeong Kim,[†] Ha-Jun Sung,[†] Woo Hyun Han,[†] In-Ho Lee,[‡] and Kee Joo Chang*[,†]

[†]Department of Physics, Korea Advanced Institute of Science and Technology, Daejeon 34141, Korea

[‡]Korea Research Institute of Standards and Science, Daejeon 34113, Korea

Supporting Information

ABSTRACT: Silicene has a two-dimensional buckled honeycomb lattice and is chemically reactive because of its mixed sp^2-sp^3 bonding character unlike graphene. Despite recent advances in epitaxial growth, it remains a great challenge to synthesize a stable silicene layer. Here, we propose an encapsulation method, in which silicene is self-encapsulated between Si(110) layers in the cubic diamond lattice and effectively protected from reaction with environmental gases. Although Si atoms are all fourfold coordinated, self-encapsulated silicene exhibits the band topology of Dirac semimetals. In a superlattice structure, in which silicene is periodically encapsulated between Si(110) layers, we also find a topological transition from a normal semiconductor to a topological nodal line semimetal as the number of Si(110) layers increases. Our results provide insights into the design of a stable silicene layer that retains the nontrivial band topology and is useful for applications of Si-based devices.

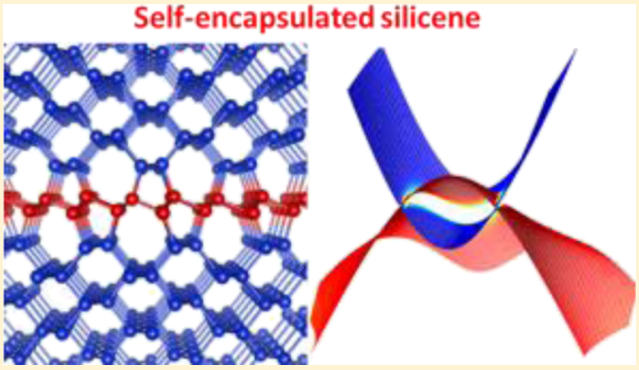

1. INTRODUCTION

Silicene, a graphene analogue for silicon, has received much attention because of its unusual physical phenomena such as quantum spin Hall effect,[1] quantum anomalous Hall effect,[2,3] chiral superconductivity,[4] and giant magnetoresistance.[5] More interestingly, silicene offers a new perspective for device applications because of its compatibility with existing semiconductor technologies.[6] As Si atoms are more advantageous for sp^3 hybridization than sp^2 hybridization, silicene has a buckled honeycomb lattice,[7,8] whereas graphene exists in a planar form of sp^2-hybridized C atoms.[9] Despite its buckled geometry, silicene belongs to the family of two-dimensional (2D) Dirac semimetals, in which quasiparticles behave as massless relativistic Dirac fermions.[8] However, an external vertical electric field breaks the sublattice symmetry of silicene and thus opens a band gap.[10] Moreover, unlike graphene, silicene is chemically sensitive to environmental gases because of its mixed sp^2-sp^3 bonding character.[11] Upon exposure to air, silicene reacts with oxygen and water molecules, degrading its electronic properties.[12,13] Hydrogenation, which fully passivates the dangling bonds, allows sp^3 hybridization and thus eliminates the Dirac points, converting silicene from a topological semimetal to a normal semiconductor.[14]

Because of the surface sensitivity, the synthesis of free-standing silicene has not yet been achieved. It is impossible to extract a single layer of silicon from bulk Si with all sp^3-hybridized bonds with a mechanical exfoliation technique. Up to now, silicene has been only epitaxially grown on various substrates such as Ag(110),[15] Ag(111),[16−18] Ir(111),[19] ZrB_2(0001),[20] and MoS_2.[21] However, silicene on metallic substrates is not suitable for device fabrication because of the difficulty of doping control in current Si-based devices. A proper choice of nonmetallic substrate is required for device applications because interfacial interactions may significantly affect the band structure of silicene, for example, removing the Dirac fermion characteristics.[22] A number of techniques using protective cladding or encapsulation layers such as NaCl,[23] AlN,[24] Al_2O_3,[12,25,26] and transition metal dichalcogenides[27] have been proposed to protect the silicene layer in air. Whereas silicene was encapsulated with NaCl and AlN, it was observed that silicene reacts with precursors via dissociative chemisorption, altering its electronic properties.[23,24] In the deposition process of Al_2O_3, a careful tailoring of Al and O_2 was necessary to prevent the oxidation of silicene via reaction with O atoms dissociated from O_2 molecules.[12,25] Even if silicene is capped with Al_2O_3, the bottom surface may degrade once the substrate is removed during the transfer process. Recently, it has been demonstrated that an encapsulated delamination technique, where both the bottom and top surfaces are protected, can preserve the characteristics of silicene at all stages from material synthesis to device fabrication.[6] Despite recent advances in epitaxial growth and

Received: October 27, 2018
Revised: January 1, 2019
Published: January 2, 2019

DOI: 10.1021/acs.jpcc.8b10475
J. Phys. Chem. C 2019, 123, 1839−1845

protection from oxidation, it is still a great challenge to fabricate a stable silicene layer for device applications.

In this work, we report a feasible way to encapsulate silicene in the cubic diamond lattice of Si. We find that a superstructure, in which silicene is self-encapsulated between Si(110) layers, exhibits the characteristics of 2D Dirac semimetals. As the number of Si(110) layers increases, the band topology changes from trivial to nontrivial. The Dirac points are protected by time-reversal and inversion symmetries, which yield the Berry phases of $\pm\pi$. In a superlattice structure, where a monolayer silicene is periodically stacked with Si(110) layers along the [110] direction, we find a similar topological transition from a normal semiconductor to a topological nodal line semimetal with increasing of the number of Si(110) layers. The self-encapsulation method not only protects the silicene layer from oxidation but also maintains the topological band characteristics, although the Si atoms are in fourfold coordination. We discuss the stability of the self-encapsulated silicene and provide a possible route to synthesizing a stable silicene layer encapsulated in the diamond lattice through wafer bonding.

2. COMPUTATIONAL DETAILS

Our first-principles calculations were performed within the framework of density functional theory, using the functional form of Perdew, Burke, and Ernzerhof (PBE) for the exchange−correlation potential[28] and the projector augmented wave potentials,[29] as implemented in the vienna ab initio simulation package code.[30] The wave functions were expanded in plane waves up to an energy cutoff of 500 eV and a k-point set with a grid spacing of $2\pi \times 0.02$ Å^{-1} was used for Brillouin zone (BZ) integration. The total energy was ensured to be accurate to within 1 meV/atom. The ionic coordinates and lattice parameters were fully relaxed with the PBE exchange−correlation functional until the residual forces and stress tensors were less than 0.01 eV/Å and 1.5 kbar, respectively.

The PBE functional usually underestimates the band gap sizes of semiconductors and insulators. Therefore, the band overlap between the valence and conduction bands may occur for systems with small band gaps. To examine whether the metallic band structure is caused by the band gap underestimation, we additionally performed more accurate calculations using the hybrid functional of Heyd, Scuseria, and Ernzerhof (HSE06) for the exchange−correlation potential,[31] which is known to improve the band gap. Here, the screening parameter (ω = 0.207 Å^{-1}) and the mixing fraction of the exact Hartree−Fock exchange (α = 0.25) were used.

3. RESULTS AND DISCUSSION

When a monolayer silicene is encapsulated in cubic diamond Si (cd-Si), the [110] direction is energetically more favorable for layer stacking than the [100] direction. Thus, we considered an encapsulated superstructure, in which a single Si(111) layer is sandwiched between the Si(110) layers with a vacuum region of ∼15 Å and the surface atoms are passivated with hydrogen, as shown in Figure 1a. The Si(111) layer has a buckled honeycomb lattice similar to silicene, and the silicene-encapsulated superstructure is denoted as $Si(110)_N/Si(111)_1/Si(110)_N$, where N is the number of Si(110) layers on each side.

In the superstructure (Figure 1a), all the Si atoms are fourfold coordinated without any coordination defects, where-

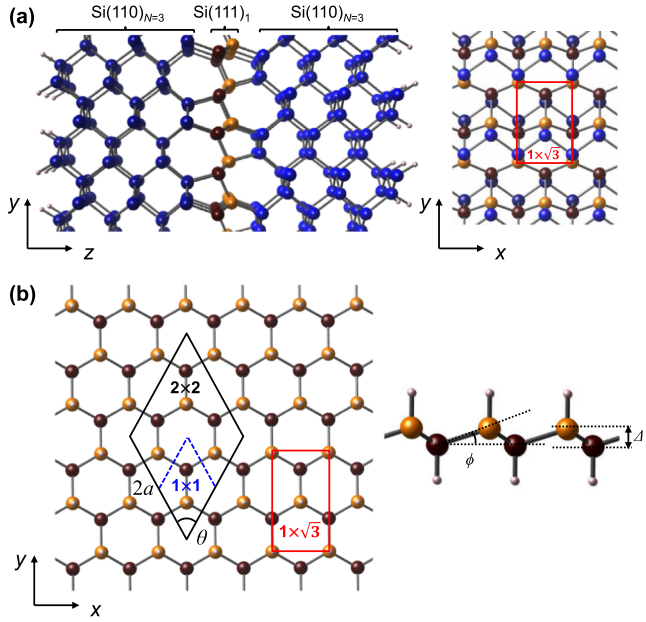

Figure 1. (a) Side view (left) of the atomic structure of the $Si(110)_3/Si(111)_1/Si(110)_3$ superstructure and top view (right) of the stacking of the atomic layers near the interface region with a primitive $1 \times \sqrt{3}$ cell on the basal plane (red rectangle). (b) Top view (left) of the atomic structure of free-standing silicene, in which the dangling bonds are passivated by hydrogen. In side view (right), Δ is the buckling height, ϕ is the buckling angle, and large and small balls represent the Si and H atoms, respectively.

as the p_z orbitals remain unsaturated in free-standing silicene. Because of different bonding orientations between the Si(110) and Si(111) layers, the interface region is composed of five- and seven-membered rings instead of six-membered rings in cd-Si (Figure S1 and Table S1). On the other hand, the Si(110) layers are well matched to the pristine cubic diamond lattice. Therefore, one can construct various superstructures by varying the number of Si(110) layers. The number of the Si(110) layers may be different on both sides of silicene (as will be discussed later), but we focus on superstructures with inversion symmetry, in which both sides have the same number of Si(110) layers.

For superstructures with $N \leq 4$, the structural properties of the encapsulated silicene are compared with those of free-standing silicene and cd-Si (Figure S2 and Table S2). The self-encapsulated silicene and free-standing silicene have different symmetries and thus different primitive cells. The superstructures have the rectangular $1 \times \sqrt{3}$ primitive cell on the basal plane, whereas the lateral primitive cell is 1×1 in free-standing silicene (Figure 1b). To directly compare the lattice constants of the superstructures and free-standing silicene, a rhombic 2×2 lateral cell was adopted for all the structures (Figure 1b). In free-standing silicene, the lattice constant is $2a$ = 7.730 Å, the angle between the two lattice vectors is $\theta = 60°$, the buckling height is Δ = 0.453 Å, and the buckling angle is ϕ = 11.48°. On the other hand, cd-Si has the smaller lattice parameter of $2a$ = 6.699 Å and the larger angle of θ = 70.53° on the (110) basal plane. Because of the lattice mismatch, the lattice parameters of superstructures lie between free-standing silicene and cd-Si and show a tendency that $2a$ decreases during the increase of θ as N increases. Therefore, the silicene layer in the superstructure is under compressive strain in the

DOI: 10.1021/acs.jpcc.8b10475
J. Phys. Chem. C 2019, 123, 1839−1845

armchair (y axis) direction, whereas the Si(110) layers are under tensile strain (Figure 1a). Moreover, both the buckling height and buckling angle are increased about twice as compared to free-standing silicene.

The $Si(110)_N/Si(111)_1/Si(110)_N$ superstructure is energetically less stable than a pristine slab structure consisting of the $(2N + 1)$ Si(110) layers. However, as all the Si atoms are fourfold coordinated like cd-Si, the excess energies are quite small, lying in the range <60 meV/atom (Table S2). The excess energy of $Si(110)_N/Si(111)_1/Si(110)_N$ tends to decrease with increasing N, with the exception of $Si(110)_1/Si(111)_1/Si(110)_1$ in which strain is effectively released by structural relaxations at the interface. For $N = 3$, we performed molecular dynamics simulations and found that the superstructure is thermally stable for up to 100 ps at a temperature of 800 K (Figure S3). Moreover, we examined the stability of $Si(110)_3/Si(111)_1/Si(110)_3$ by calculating the full phonon spectra and found no imaginary phonon modes, identifying that the superstructure is dynamically stable (Figure S3).

The band structures of $Si(110)_N/Si(111)_1/Si(110)_N$ are shown for $N \leq 4$ in the 2D BZ of the primitive cell (Figure 2a–c). The superstructures with $N = 1$ and 2 are trivial

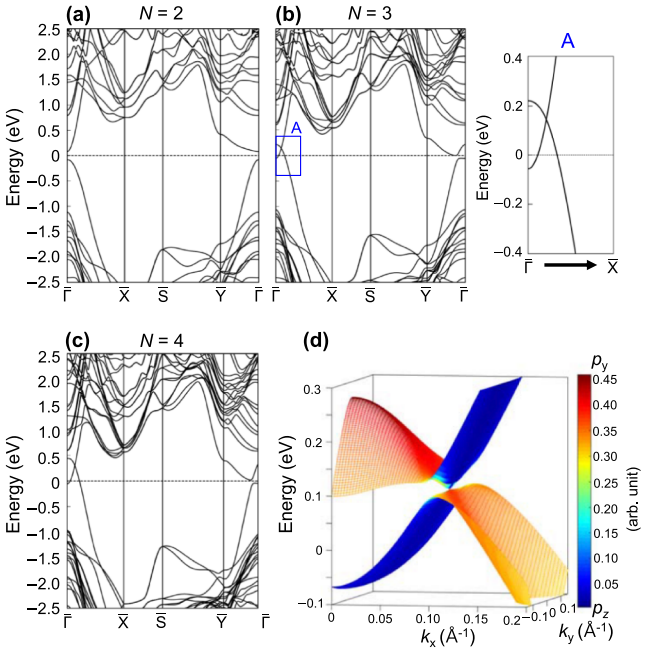

Figure 2. (a–c) HSE06 band structures of $Si(110)_N/Si(111)_1/Si(110)_N$ superstructures with $2 \leq N \leq 4$. For $N = 3$, a magnified view of the band inversion near the $\bar{\Gamma}$ point is shown in (b) and the orbital characteristics of the band edge states around the Dirac point are plotted in (d). See Figure 3a for the symmetry points in the 2D BZ.

insulators with the band gaps of 1.18 and 0.16 eV, respectively. As N increases, the band gap tends to decrease. With the HSE06 functional, we find that the band overlap occurs for $N \geq 3$, with two band crossing points along the $\bar{\Gamma} - \bar{X}$ line. In order to confirm whether the semimetallic band structure is caused by band inversion, we analyzed the orbital characteristics of the band edge states (Figure S4). The isosurfaces of the charge densities show that the band edge states are associated with the silicene layer. For $N = 2$, the Si p_y bonding orbitals of the silicene layer are dominant for the valence band maximum (VBM) state, whereas the conduction band minimum (CBM) state mainly comprises the Si p_z orbitals. For $N = 3$, the orbital characteristics of the band edge states are reversed (Figure 2d), supporting the band inversion between the VBM and CBM states around the $\bar{\Gamma}$ point.

To understand the origin of the band inversion, we examined the effect of strain (ε) on the band structure of free-standing hydrogenated silicene (H-silicene), which corresponds to the $N = 0$ superstructure. The band structure of H-silicene is drawn for the BZ of the rectangular $1 \times \sqrt{3}$ cell to compare with those of superstructures. Therefore, the $\bar{M}'$ point in the BZ of the 1×1 cell is folded to the $\bar{\Gamma}$ point (Figure 3a).

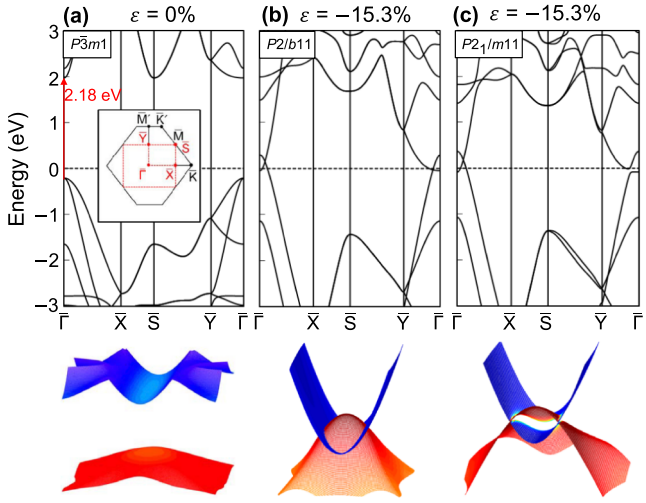

Figure 3. Folded band structure of (a) pristine H-silicene and (b) H-silicene under −15.3% strain. The inset shows the BZ folding as the rhombic 1×1 cell (black) converts to the rectangular $1 \times \sqrt{3}$ cell (red). (c) Effect of symmetry-breaking relaxations on the band structure of strained H-silicene ($\varepsilon = -15.3\%$). In lower panels, the evolution of band structure near the Fermi energy is drawn as the layer group changes from $P\bar{3}m1$ to $P2/b11$ and then to $P2_1/m11$.

Upon hydrogenation, the buckling height and buckling angle significantly increase to 0.718 Å and 18.08°, respectively (Table S2). Moreover, because of the sp^3-hybridized bonds, the Dirac points formed by the p_z orbitals are removed, yielding a band gap of 2.18 eV (Figure 3a). The degenerate VBM states at the $\bar{\Gamma}$ point are characterized by the in-plane p_x and p_y orbitals, whereas the CBM state has the characteristics of the p_z orbitals. Under compressive strain along the y axis, the degeneracy of the VBM states is lifted by the symmetry breaking between the p_x and p_y orbitals. Then, the band edge states have the orbital characteristics similar to those of $Si(110)_2/Si(111)_1/Si(110)_2$.

In the superstructure, the compressive strain acting on the silicene layer increases with increasing N because the Si(110) layers are more rigid. For $N = 3$, the compressive strain is estimated to be −15.3% as compared to H-silicene. As the arrangement of five- and seven-membered rings is asymmetric at the interface, different buckling relaxations occur for the Si atoms, depending on whether the Si atoms share two five-membered or two seven-membered rings. This symmetry-breaking relaxation yields two buckling heights of 0.846 and 1.065 Å (average Δ value = 0.956 Å) and two buckling angles of 22.52° and 22.56° (average ϕ value = 22.54°) (Table S2). As the compressive strain increases, the bonding between the p_y orbitals is weakened and the VBM state increases. On the

DOI: 10.1021/acs.jpcc.8b10475
J. Phys. Chem. C 2019, 123, 1839–1845

other hand, the CBM state is lowered because of the enhanced coupling of the antibonding orbitals along the y axis. Therefore, overall the band gap is reduced under compressive strain. In fact, when H-silicene is under the same compressive strain ($\varepsilon = -15.3\%$), we observed the band inversion around the $\bar{\Gamma}$ point (Figure 3b). In this case, the buckling angle is 22.87°, comparable to that of $Si(110)_3/Si(111)_1/Si(110)_3$, whereas the buckling height of 0.867 Å is slightly smaller. This result indicates that the band inversion for the superstructures with $N \geq 3$ results from the enhanced buckling angle of the silicene layer by compressive strain.

The $Si(110)_N/Si(111)_1/Si(110)_N$ superstructure with the $P2_1/m11$ (no. 15) layer group has both time-reversal and inversion symmetries. In H-silicene with the $P\bar{3}m1$ (no. 72) layer group, all the Si atoms have the same buckling height and buckling angle, so additional symmetries exist, such as 180° rotation about the x axis (C_{2x}), 120° rotation about the z axis (C_{3z}), and mirror reflection with respect to the yz plane (M_x). When the C_{3z} symmetry is broken under compressive strain along the y axis, the layer group changes to $P2/b11$ (no. 16). If the compressive strain is large enough to induce the band inversion, the band crossing points form a nodal ring around the $\bar{\Gamma}$ point in the folded BZ (Figure 3b). If two different buckling heights are intentionally introduced to the strained H-silicene, the C_{2x} symmetry breaks further and the layer group is the same as that of the superstructure. The band gap then opens along the nodal ring, except for two crossing points on the $\bar{\Gamma} - \bar{X}$ line (Figure 3c). We calculated Berry phases along two independent circular loops related to the Dirac points using maximally localized Wannier functions,[32] which reproduce the band structure of strained H-silicene. The Berry phases were found to be $\pm\pi$, implying that quasiparticles are massless Dirac fermions with the pseudospin 1/2 (Figure S5). For various nanoribbons of the strained H-silicene with different ribbon widths, we find one-dimensional edge states, similar to other 2D Dirac semimetals such as graphene and free-standing silicene (Figure S6).[8,33] In the $N = 3$ superstructure, we actually find two Dirac points on the $\bar{\Gamma} - \bar{X}$ line, which are protected by inversion and time-reversal symmetries. Because of the presence of the M_x symmetry, the two Dirac points are located along the high symmetry line of $k_y = 0$. With including the spin−orbit coupling (SOC), it is not sufficient to protect the Dirac points because the superstructure does not have either nonsymmorphic symmetry or rotational symmetries such as C_3, C_4, and C_6.[34] Nevertheless, it can be seen that the spin−orbit gap (~1 meV) is very small because of the weak SOC in the current Si system.[35] When the numbers of the Si(110) layers on both sides of silicene are different, the inversion symmetry is broken, opening the band gap at the Dirac point even in the absence of the SOC (Table S3).

We examined the band topology of the $Si(110)_N/Si(111)_1/Si(110)_N$ superstructure by calculating the Z_2 topological invariant ν, in which $\nu = 0$ and $\nu = 1$ indicate the trivial and nontrivial states, respectively.[36,37] As the inversion symmetry exists in all the superstructures, the Z_2 invariant in 2D can be calculated by the product of the parity eigenvalues for the occupied bands (δ) at four time-reversal invariant momentum (TRIM) points, $\bar{\Gamma}$, $\bar{N}$, $\bar{N}'$, and $\bar{Y}$ in 2D BZ (Table S4). The HSE06 calculations show that the Z_2 index is $\nu = 0$ for $N = 1$ and 2; therefore, these superstructures are trivial insulators. For $N = 3$ and 4, we find the topological Z_2 index of $\nu = 1$, indicating that both the superstructures are 2D Dirac semimetals.

A silicene-encapsulated superlattice structure can be made by periodically stacking a monolayer silicene with the Si(110) layers along the [110] direction (Figure 4a). Then, one can

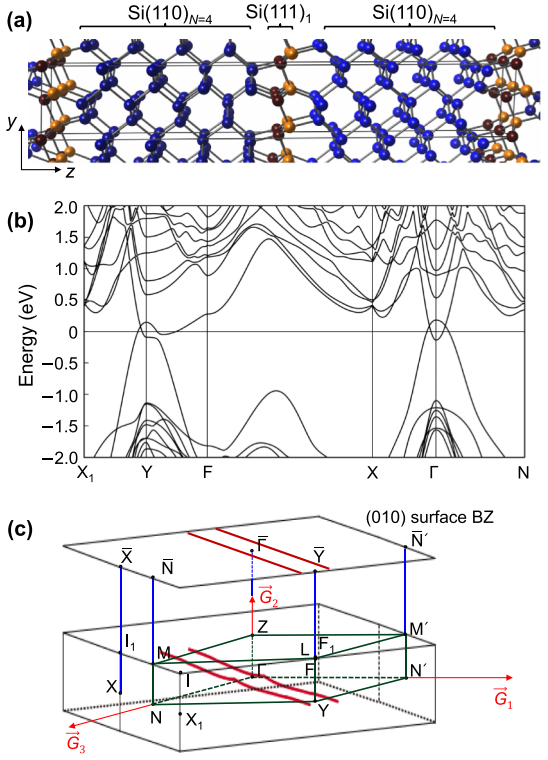

Figure 4. (a) Atomic structure, (b) HSE06 band structure, and (c) topological nodal lines (red) in the bulk BZ of $Si(110)_4/Si(111)_1$-SL. Eight TRIM points are indicated at the vertices of green parallelepiped and the projection of the nodal lines onto the (010) surface BZ are shown in (c). The coordinates of high symmetry points in the monoclinic BZ are given in Table S6.

expect that the Dirac points are connected in the reciprocal space. We generalize the superlattice structure [denoted as $Si(110)_N/Si(111)_1$-SL with the $C2/m$ space group] by varying the number of Si(110) layers. In fact, we explored new allotropes with low energies and small gaps using an *ab initio* evolutionary crystal structure search method, as implemented in the AMADEUS code.[38] In this approach, the conformational space-annealing algorithm for global optimization is combined with first-principles density functional calculations. Especially for the system containing 24 atoms per unit cell, we found a very distinctive allotrope, which is equivalent to the $Si(110)_2/Si(111)_1$-SL structure. Similar to superstructures, the lattice parameters of $Si(110)_N/Si(111)_1$-SL lie between free-standing silicene and cd-Si and their excess energies are in the range of <90 meV/atom (Table S5). Because of compressive strain, the silicene layers also show a tendency that the buckling height and buckling angle increase with increasing N. As the buckling relaxations of silicene are less significant, the band inversion between the CBM and VBM states was observed for $N \geq 4$ around the Γ and Y points in the three-dimensional (3D) BZ (Figures 4b and S7). The band topology of $Si(110)_N/Si(111)_1$-SL was examined by calculating the Z_2 topological invariant (ν_0; $\nu_1\nu_2\nu_3$) in 3D, which was proposed to describe the characteristics of topological insulators.[36,37] The products of the parity eigenvalues for the occupied bands are calculated for eight

DOI: 10.1021/acs.jpcc.8b10475
J. Phys. Chem. C 2019, 123, 1839−1845

TRIM points in 3D BZ (Table S6). The HSE06 calculations show that the Z_2 index is $(\nu_0; \nu_1\nu_2\nu_3) = (0; 000)$ for $N = 1$, 2, and 3; therefore, these superlattices are trivial insulators. For $N = 4$ and 5, we find the weak topological Z_2 index of $(\nu_0; \nu_1\nu_2\nu_3) = (0; 101)$, indicating that both the superlattices are topological semimetals.

For the $N = 4$ superlattice, we find that the crossing points between the valence and conduction bands form a continuous nodal line in the full BZ, as shown in Figure 4. Similar to the superstructure, the SOC opens a small band gap at the band crossing points in the superlattice. However, because the SOC is negligible, the topological nodal lines can survive by the combination of inversion and time-reversal symmetries, as addressed in other nodal line semimetals such as Ca_3P_2, Cu_3PdN, and LaN.[39−42] Therefore, the $N = 4$ superlattice belongs to the class of topological nodal line semimetals. To find the topological surface states, we calculated the surface band structure for a slab geometry with a thickness of 55.58 Å. We employed the PBE functional for the exchange−correlation potential because of the high computational demand with the HSE06 hybrid functional. The (010) surface of the superlattice is exposed to vacuum and the surface dangling bonds are passivated by hydrogen. As the nodal lines are parallel to the $\Gamma - Y$ line, the topological surface states can be visualized around the $\bar{\Gamma}$ and $\bar{Y}$ points when the bulk BZ is projected onto the (010) surface BZ. The projected band structure is drawn along the $\bar{\Gamma} - \bar{X}$ line, and the formation of the nearly flat surface band is seen around the $\bar{\Gamma}$ point (Figure S8). The surface states are well localized near the surface region, although they are located far from the Fermi level because the band gap of the Si(110) layers of cd-Si is underestimated and the nodal line lies in the bulk conduction bands.

Finally, we discuss the synthesis of a silicene layer inserted in the cubic diamond lattice. For the Si(110) surface, it was reported that the 16 × 2 reconstructed surface is the most stable structure.[43−45] When Au atoms are adsorbed on the Si(110) surface, various surface structures can be formed, such as 16 × 2, 1 × 1, 1 × 2, and 2 × 5 reconstructions.[46] Especially, with a half monolayer coverage of Au at temperatures lower than 440 °C, the (110) surface forms the 1 × 1 structure. On the clean Si(110) 1 × 1 surface, the surface zigzag chains are tilted by an angle of 31.8° from the surface layer. When a half monolayer of Au is deposited on the (110) surface, the Au atoms are adsorbed at hollow sites, and the surface zigzag chains become almost parallel to the surface plane (Figure S9). Recently, a silicene filed-effect transistor has been demonstrated using an encapsulated delamination technique that can protect the bottom and top surfaces.[6] This technique can be used to replace the substrate material while preserving the characteristics of silicene after synthesis on the Ag surface. If a silicene layer is sandwiched between two Au-deposited Si(110) 1 × 1 surfaces, silicene is under compressive strain because of the lattice mismatch between the silicene and Si(110) surface. The variation of the total energy is plotted as a function of the separation between the two Si(110) surfaces (Figure S9). We find no energy barrier for forming the interface. Once the interface is formed, the Au atoms can be removed through a degassing process at elevated temperatures, which was successfully used for a chemical precursor $NaSi_6$ to obtain an orthorhombic Si_6 clathrate.[47] We examined the migration of Au along the open channel in the interface region and estimated the migration barrier to be about 0.14 eV/atom using a climbing image nudged elastic band method.[48] Because of the small migration barrier of Au, the wafer bonding can serve as a useful technique for encapsulating a silicene layer in the cubic diamond lattice.

4. CONCLUSIONS

In conclusion, we have proposed a self-encapsulation method to fabricate a stable silicene layer in the cubic diamond lattice of Si. Although the Si atoms are fourfold coordinated, the encapsulated silicene exhibits the nontrivial band topology, belonging to the family of 2D Dirac semimetals. The Dirac points are created by the strain-induced band inversion and protected by the presence of time-reversal and inversion symmetries. Although the SOC opens a band gap at the Dirac points, the spin−orbit gap is very small in the present Si system. In the superlattice structure, in which a monolayer silicene and a few Si(110) layers are alternately stacked along the [110] direction, the electronic structure evolves from a normal semiconductor to a topological nodal line semimetal as the number of the Si(110) layers increases. We have identified the formation of the Fermi arc states connecting the projected nodal points at the surface. We have shown that a single silicene layer can be encapsulated in the cubic diamond lattice through wafer bonding to be effectively protected from oxidation in the air.

■ ASSOCIATED CONTENT

Supporting Information

The Supporting Information is available free of charge on the ACS Publications website at DOI: 10.1021/acs.jpcc.8b10475.

Details of the lattice parameters, dynamical and thermal stability, orbital projected band structure, Berry curvature, edge and surface states, band structures for superlattices, and wafer bonding effect (PDF)

■ AUTHOR INFORMATION

Corresponding Author

*E-mail: kjchang@kaist.ac.kr.

ORCID

Woo Hyun Han: 0000-0001-9575-5868

Kee Joo Chang: 0000-0002-5364-8551

Author Contributions

G.-M.K., H.-J.S., and W.H.H. performed theoretical calculations and data analysis and participated in the article preparation. All the authors contributed to the scientific discussion. K.J.C. conducted the research, performed data analysis, and participated in the article preparation.

Notes

The authors declare no competing financial interest.

■ ACKNOWLEDGMENTS

This work was supported by the Samsung Science and Technology Foundation under grant no. SSTF-BA1401-08.

■ REFERENCES

(1) Liu, C.-C.; Feng, W.; Yao, Y. Quantum Spin Hall Effect in Silicene and Two-Dimensional Germanium. *Phys. Rev. Lett.* **2011**, *107*, 076802.

(2) Ezawa, M. Valley-Polarized Metals and Quantum Anomalous Hall Effect in Silicene. *Phys. Rev. Lett.* **2012**, *109*, 055502.

(3) Pan, H.; Li, Z.; Liu, C.-C.; Zhu, G.; Qiao, Z.; Yao, Y. Valley-Polarized Quantum Anomalous Hall Effect in Silicene. *Phys. Rev. Lett.* **2014**, *112*, 106802.

DOI: 10.1021/acs.jpcc.8b10475
J. Phys. Chem. C 2019, 123, 1839−1845

(4) Liu, F.; Liu, C.-C.; Wu, K.; Yang, F.; Yao, Y. d+id' Chiral Superconductivity in Bilayer Silicene. *Phys. Rev. Lett.* **2013**, *111*, 066804.
(5) Xu, C.; Luo, G.; Liu, Q.; Zheng, J.; Zhang, Z.; Nagase, S.; Gao, Z.; Lu, J. Giant magnetoresistance in silicene nanoribbons. *Nanoscale* **2012**, *4*, 3111−3117.
(6) Tao, L.; Cinquanta, E.; Chiappe, D.; Grazianetti, C.; Fanciulli, M.; Dubey, M.; Molle, A.; Akinwande, D. Silicene field-effect transistors operating at room temperature. *Nat. Nanotechnol.* **2015**, *10*, 227−231.
(7) Takeda, K.; Shiraishi, K. Theoretical possibility of stage corrugation in Si and Ge analogs of graphite. *Phys. Rev. B: Condens. Matter Mater. Phys.* **1994**, *50*, 14916.
(8) Cahangirov, S.; Topsakal, M.; Aktürk, E.; Şahin, H.; Ciraci, S. Two- and One-Dimensional Honeycomb Structures of Silicon and Germanium. *Phys. Rev. Lett.* **2009**, *102*, 236804.
(9) Novoselov, K. S.; Geim, A. K.; Morozov, S. V.; Jiang, D.; Katsnelson, M. I.; Grigorieva, I. V.; Dubonos, S. V.; Firsov, A. A. Two-dimensional gas of massless Dirac fermions in graphene. *Nature* **2005**, *438*, 197−200.
(10) Drummond, N. D.; Zólyomi, V.; Fal'ko, V. I. Electrically tunable band gap in silicene. *Phys. Rev. B: Condens. Matter Mater. Phys.* **2012**, *85*, 075423.
(11) Cinquanta, E.; Scalise, E.; Chiappe, D.; Grazianetti, C.; van den Broek, B.; Houssa, M.; Fanciulli, M.; Molle, A. Getting through the Nature of Silicene: An sp^2−sp^3 Two-Dimensional Silicon Nanosheet. *J. Phys. Chem. C* **2013**, *117*, 16719−16724.
(12) Molle, A.; Grazianetti, C.; Chiappe, D.; Cinquanta, E.; Cianci, E.; Tallarida, G.; Fanciulli, M. Hindering the Oxidation of Silicene with Non-Reactive Encapsulation. *Adv. Funct. Mater.* **2013**, *23*, 4340−4344.
(13) Wang, R.; Pi, X.; Ni, Z.; Liu, Y.; Lin, S.; Xu, M.; Yang, D. Silicene oxides: formation, structures and electronic properties. *Sci. Rep.* **2013**, *3*, 3507.
(14) Trivedi, S.; Srivastav, A.; Kurchania, R. Silicene and Germanene: A First Principle Study of Electronic Structure and Effect of Hydrogenation-Passivation. *J. Comput. Theor. Nanosci.* **2014**, *11*, 781.
(15) Aufray, B.; Kara, A.; Vizzini, S.; Oughaddou, H.; Léandri, C.; Ealet, B.; Le Lay, G. Graphene-like silicon nanoribbons on Ag(110): A possible formation of silicene. *Appl. Phys. Lett.* **2010**, *96*, 183102.
(16) Le Lay, B.; Oughaddou, H.; Enriquez, H.; Kara, A.; Vizzini, S.; Ealet, B.; Aufray, B. Epitaxial growth of a silicene sheet. *Appl. Phys. Lett.* **2010**, *97*, 223109.
(17) Vogt, P.; De Padova, P.; Quaresima, C.; Avila, J.; Frantzeskakis, E.; Asensio, M. C.; Resta, A.; Ealet, B.; Le Lay, G. Silicene: Compelling Experimental Evidence for Graphenelike Two-Dimensional Silicon. *Phys. Rev. Lett.* **2012**, *108*, 155501.
(18) Feng, B.; Ding, Z.; Meng, S.; Yao, Y.; He, X.; Cheng, P.; Chen, L.; Wu, K. Evidence of Silicene in Honeycomb Structures of Silicon on Ag(111). *Nano Lett.* **2012**, *12*, 3507−3511.
(19) Meng, L.; Wang, Y.; Zhang, L.; Du, S.; Wu, R.; Li, L.; Zhang, Y.; Li, G.; Zhou, H.; Hofer, W. A.; et al. Buckled Silicene Formation on Ir(111). *Nano Lett.* **2013**, *13*, 685−690.
(20) Fleurence, A.; Friedlein, R.; Ozaki, T.; Kawai, H.; Wang, Y.; Yamada-Takamura, Y. Experimental Evidence for Epitaxial Silicene on Diboride Thin Films. *Phys. Rev. Lett.* **2012**, *108*, 245501.
(21) Chiappe, D.; Scalise, E.; Cinquanta, E.; Grazianetti, C.; van den Broek, B.; Fanciulli, M.; Houssa, M.; Molle, A. Two-Dimensional Si Nanosheets with Local Hexagonal Structure on a MoS_2 Surface. *Adv. Mater.* **2013**, *26*, 2096−2101.
(22) Guo, Z.-X.; Furuya, S.; Iwata, J.-I.; Oshiyama, A. Absence and presence of Dirac electrons in silicene on substrates. *Phys. Rev. B: Condens. Matter Mater. Phys.* **2013**, *87*, 235435.
(23) Wiggers, F. B.; Yamada-Takamura, Y.; Kovalgin, A. Y.; de Jong, M. P. Encapsulation of epitaxial silicene on ZrB_2 with NaCl. *J. Chem. Phys.* **2017**, *147*, 064701.
(24) Van Bui, H.; Wiggers, F. B.; Friedlein, R.; Yamada-Takamura, Y.; Kovalgin, A. Y.; de Jong, M. P. On the feasibility of silicene encapsulation by AlN deposited using an atomic layer deposition process. *J. Chem. Phys.* **2015**, *142*, 064702.
(25) Friedlein, R.; Van Bui, H.; Wiggers, F. B.; Yamada-Takamura, Y.; Kovalgin, A. Y.; de Jong, M. P. Interaction of epitaxial silicene with overlayers formed by exposure to Al atoms and O_2 molecules. *J. Chem. Phys.* **2014**, *140*, 204705.
(26) Molle, A.; Chiappe, D.; Cinquanta, E.; Grazianetti, C.; Fanciulli, M.; Scalise, E.; van den Broek, B.; Houssa, M. (Invited) Structural and Chemical Stabilization of the Epitaxial Silicene. *ECS Trans.* **2013**, *58*, 217−227.
(27) Kou, L.; Ma, Y.; Yan, B.; Tan, X.; Chen, C.; Smith, S. C. Encapsulated Silicene: A Robust Large-Gap Topological Insulator. *ACS Appl. Mater. Interfaces* **2015**, *7*, 19226−19233.
(28) Perdew, J. P.; Burke, K.; Ernzerhof, M. Generalized Gradient Approximation Made Simple. *Phys. Rev. Lett.* **1996**, *77*, 3865.
(29) Blöchl, P. E. Projector augmented-wave method. *Phys. Rev. B: Condens. Matter Mater. Phys.* **1994**, *50*, 17953.
(30) Kresse, G.; Furthmüller, J. Efficient iterative schemes forab initiototal-energy calculations using a plane-wave basis set. *Phys. Rev. B: Condens. Matter Mater. Phys.* **1996**, *54*, 11169.
(31) Heyd, J.; Scuseria, G. E.; Ernzerhof, M. Hybrid functionals based on a screened Coulomb potential. *J. Chem. Phys.* **2003**, *118*, 8207.
(32) Mostofi, A. A.; Yates, J. R.; Lee, Y.-S.; Souza, I.; Vanderbilt, D.; Marzari, N. Wannier90: A tool for obtaining maximally-localised Wannier functions. *Comput. Phys. Commun.* **2008**, *178*, 685−699.
(33) Nakada, K.; Fujita, M.; Dresselhaus, G.; Dresselhaus, M. S. Edge state in graphene ribbons: Nanometer size effect and edge shape dependence. *Phys. Rev. B: Condens. Matter Mater. Phys.* **1996**, *54*, 17954−17961.
(34) Young, S. M.; Kane, C. L. Dirac Semimetals in Two Dimensions. *Phys. Rev. Lett.* **2015**, *115*, 126803.
(35) Liu, C.-C.; Jiang, H.; Yao, Y. Low-energy effective Hamiltonian involving spin-orbit coupling in silicene and two-dimensional germanium and tin. *Phys. Rev. B: Condens. Matter Mater. Phys.* **2011**, *84*, 195430.
(36) Fu, L.; Kane, C. L.; Mele, E. J. Topological Insulators in Three Dimensions. *Phys. Rev. Lett.* **2007**, *98*, 106803.
(37) Fu, L.; Kane, C. L. Topological insulators with inversion symmetry. *Phys. Rev. B: Condens. Matter Mater. Phys.* **2007**, *76*, 045302.
(38) Lee, I.-H.; Oh, Y. J.; Kim, S.; Lee, J.; Chang, K. J. *Ab initio* materials design using conformational space annealing and its application to searching for direct band gap silicon crystals. *Comput. Phys. Commun.* **2016**, *203*, 110−121.
(39) Fang, C.; Chen, Y.; Kee, H.-Y.; Fu, L. Topological nodal line semimetals with and without spin-orbital coupling. *Phys. Rev. B: Condens. Matter Mater. Phys.* **2015**, *92*, 081201.
(40) Xie, L. S.; Schoop, L. M.; Seibel, E. M.; Gibson, Q. D.; Xie, W.; Cava, R. J. A new form of Ca_3P_2 with a ring of Dirac nodes. *APL Mater.* **2015**, *3*, 083602.
(41) Yu, R.; Weng, H.; Fang, Z.; Dai, X.; Hu, X. Topological node-line semimetal and Dirac semimetal state in antiperovskite Cu_3PdN. *Phys. Rev. Lett.* **2015**, *115*, 036807.
(42) Zeng, M.; Fang, C.; Chang, G.; Chen, Y.-A.; Hsieh, T.; Bansil, A.; Lin, H.; Fu, L. Topological semimetals and topological insulators in rare earth monopnitides. arXiv :1504.03492 2015.
(43) Ampo, H.; Miura, S.; Kato, K.; Ohkawa, Y.; Tamura, A. Atomic configuration of hydrogenated and clean Si(110) surfaces. *Phys. Rev. B: Condens. Matter Mater. Phys.* **1986**, *34*, 2329.
(44) An, T.; Yoshimura, M.; Ono, I.; Ueda, K. Elemental structure in Si(110)-″16×2″ revealed by scanning tunneling microscopy. *Phys. Rev. B: Condens. Matter Mater. Phys.* **2000**, *61*, 3006.
(45) Yamasaki, T.; Kato, K.; Uda, T.; Yamamoto, T.; Ohno, T. First-principles theory of Si(110)-(16 × 2) surface reconstruction for unveiling origin of pentagonal scanning tunneling microscopy images. *Appl. Phys. Express* **2016**, *9*, 035501.
(46) Yamamoto, Y. RHEED-TRAXS study of superstructures induced by Au on a Si(110) surface. *Surf. Sci.* **1992**, *271*, 407.

DOI: 10.1021/acs.jpcc.8b10475
J. Phys. Chem. C 2019, 123, 1839−1845

(47) Kim, D. Y.; Stefanoski, S.; Kurakevych, O. O.; Strobel, T. A. Synthesis of an open-framework allotrope of silicon. *Nat. Mater.* **2014**, *14*, 169.
(48) Henkelman, G.; Uberuaga, B. P.; Jónsson, H. A climbing image nudged elastic band method for finding saddle points and minimum energy paths. *J. Chem. Phys.* **2000**, *113*, 9901.

DOI: 10.1021/acs.jpcc.8b10475
J. Phys. Chem. C 2019, 123, 1839−1845